Electron-energy losses in silicon: Bulk and surface plasmons and Čerenkov radiation*

C. H. Chen, J. Silcox, and R. Vincent
School of Applied and Engineering Physics, Clark Hall, Cornell University, Ithaca, New York 14850
(Received 17 October 1973; revised manuscript received 15 October 1974)

Characteristic electron-energy-loss processes in crystalline silicon foils are examined for scattering angles less than 2.5×10^{-4} rad. The relatively high energy of the electron beam (75 keV), combined with a low angular divergence (8×10^{-6} rad), allows identification of retardation effects in both volume and surface excitations. The results are consistent with complete probability distribution maps, calculated as a function of energy loss $\hbar\omega$ and scattering angle θ, using recent optical data for the dielectric constants of Si. The half-width of the angular intensity distribution in the volume plasmon ($\hbar\omega_p = 16.6$ eV) agrees with the theoretical value to within 3%. Below 4 eV ($\epsilon_1 > 10$), a dispersive peak in the loss spectrum is observed which is interpreted as a volume loss due to Čerenkov radiation for $\theta \geq 5 \times 10^{-5}$ rad, and which, at small angles, transforms into multiple surface modes propagating parallel to the specimen surface in a waveguide fashion. Between 4.3 eV and $\hbar\omega_p = 16.6$ eV (ϵ_1 negative), the prominent excitation is the surface plasmon in which the wave fields decay exponentially on both sides of the surface. The dispersion follows the light line and then approaches an asymptotic energy (8.2 eV) which is less than the energy calculated for a clean Si surface ($\hbar\omega_s = 11.0$ eV), but dispersion curves calculated for 20- and 50-Å SiO_x ($x \approx 1.5$) approximately fit the data.

I. INTRODUCTION

In the long-wavelength limit,[1] the semiclassical dielectric theory[2-4] is expected to give an essentially complete description of the energy $\hbar\omega$ lost by fast electrons passing through a thin slab of material, provided that corrections are made for multiple energy losses, elastic scattering, and the limitations of instrumental resolution. At small scattering angles θ, it is important to use the complete set of Maxwell equations[3] when calculating the energy-loss probability function because retardation effects due to the finite velocity of light change the dispersion of surface excitations. Ultimately, the complex dielectric constant $\epsilon(\omega) = \epsilon_1(\omega) - i\epsilon_2(\omega)$; $\epsilon_2(\omega) > 0$, is sufficient to characterize the dispersion, damping, and excitation probability of all energy-loss processes. For metals where the dielectric constant resembles the free-electron (Drude) model over a particlar range of ω, the behavior of the surface plasmon in the vicinity of the light line is reasonably well understood. Experimental measurements[5,6] confirm that, for $\epsilon_1 \leq -1$, there exist well-defined solutions for the dispersion equation which are asymptotic to the light line $\omega = ck_s$ as k_s tends to zero. k_s is the wave vector of the surface excitation—in this case the surface plasmon. Charge oscillations are localized at the surface, with wave fields decaying exponentially away from the surfaces both in vacuum and in the slab. Considering the electric field component parallel to the surface, symmetric and antisymmetric modes can be identified with mode frequencies ω^- and ω^+, respectively, which are almost equal and independent of thickness for thick films (> 300 Å for Al).

The dielectric constants for semiconductors (e.g. Si, Ge, and the III-V compounds GaP and GaAs) represent a further stage of complexity beyond the free-electron case. For silicon, the oscillator strength for transitions from the valence band to the conduction band is quite weak above 10 eV, and so the dielectric constants approximate free-electron behavior[7]; the plasmon resonance energy occurs at 16.6 ± 0.1 eV.[8] Below 4 eV, ϵ_1 is large and positive, with a peak value of 44 at 3.4 eV.[9] The absorption edge is clearly seen in ϵ_2, which rises rapidly above 3 eV. Previous optical[10] and electron-energy-loss[11,12] experiments have confirmed that fast electrons traversing a thin foil may lose energy by Čerenkov radiation[2,13] if ϵ_1 is sufficiently large. The initial purpose of the present experiments was to verify the dispersion of the Čerenkov loss at small scattering angles. However, complete theoretical calculations including the effect of surface terms show that the energy-loss probability function becomes a complex mixture of volume and surface losses. For a semiconductor slab in a vacuum with $\epsilon_1^{1/2} > ck_s/\omega > 1$ and $\epsilon_2 \sim 0$, the wave fields associated with surface-charge oscillations are sinusoidal in the slab but decay exponentially into the vacuum. In this case standing waves are set up in the dielectric. Families of symmetric and antisymmetric modes again occur with mode frequencies ω_g^- and ω_g^+, and have associated thickness-dependent dispersion curves. The separation between modes persists to much greater thickness than in the case of the surface plasmon. These excitations correspond to the multiple nonradiative solutions considered by Kliewer and Fuchs[14] for undamped optical modes of vibration in an ionic crystal slab. Likewise, the theo-

retical contour maps calculated by Kröger[2] for GaP contain several peaks which are identified as multiple surface excitations.

In silicon, electron-energy losses should therefore show these effects together with surface- and bulk-plasmon losses, provided sufficiently high angular resolution is attained. The present measurements on thick Si foils are interpreted in terms which should be generally applicable to any isotropic material.

II. EXPERIMENTAL

Electron-transparent specimens were made by chemical thinning[15] of single-crystal (111) wafers of high-purity silicon. Estimates made by counting thickness fringes indicate that the thickness typically varied from 1000 to 2000 Å over the area illuminated by the electron beam (~0.1-mm diam). Although the silicon flakes were thoroughly washed before transfer to the electron spectrometer, no special precautions were taken to prevent oxidation; specimens were exposed to the atmosphere for at least 15 min.

The resolution and operation of the apparatus is described in detail elsewhere.[16] Briefly, an electron microscope is used to provide a beam with low divergence at the specimen (8×10^{-6} rad at 75 keV). The effective camera length is 25 m at the entrance to a Wien filter spectrometer mounted below the microscope column. Photographic plates are used to record the focussed dispersive image of the electron distribution along the entrance slit. The image formed in this way is directly related to the energy-loss probability function, subject to the instrumental and theoretical limitations mentioned above. The energy resolution is limited mainly by the thermal spread in the incident beam. For long exposure times (15 min), the width of the zero-loss line, containing the phonon-scattered and elastically scattered electrons, is ~0.7 eV. Numerical data were obtained from the photographic plates by the use of a Joyce-Loebl Mk III C automatic recording densitometer.

III. ENERGY-LOSS SPECTRA

Figures 1(a) and 1(b) illustrate the energy-loss spectra at normal incidence, and Fig. 1(c) is a sketch of the main features with identification according to the theory discussed in detail in Sec. IV. The two horizontal lines correspond to bulk plasmon excitation and to phonon and elastic scattering. Over the range of the angles considered here the bulk plasmon has negligible dispersion. The dispersion of the surface plasmon follows the light line closely at small k_s and then goes to an asymptotic energy $\hbar\omega_s$ at large k_s as expected. We identify the remaining loss as due to the excitation of Cerenkov radiation. To a first approximation, the

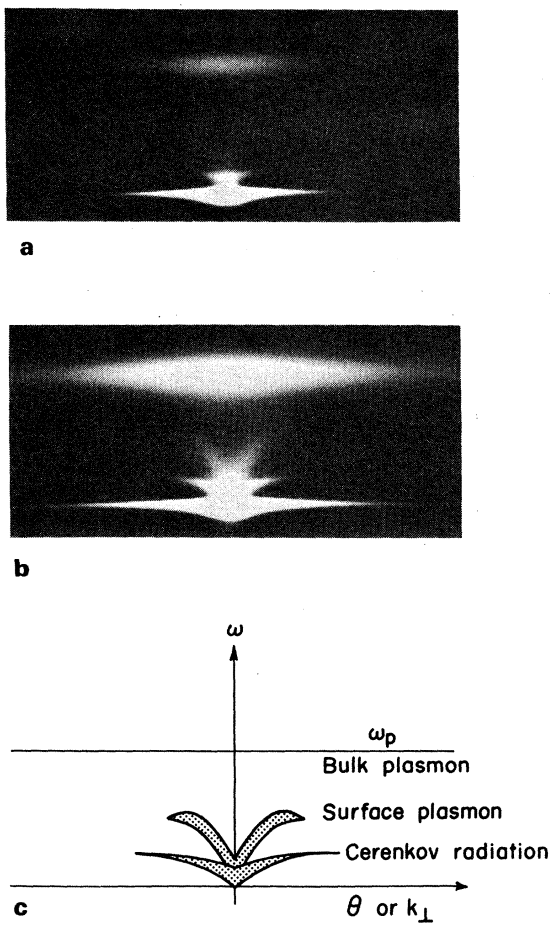

FIG. 1. Electron-energy-loss spectra in silicon at normal incidence. (a) Spectrum taken at lower exposure time (~4 min), in order to see the details close to the origin; (b) spectrum taken at longer exposure time (~10 min); (c) a sketch of main features shown in (a) and (b) with identification of losses. The horizontal line passing through the central spot ($\hbar\omega=0$) contains electrons scattered by elastic collisions and by phonons.

dependence of this loss on scattering angle arises from the dispersion relation of light in an infinite dielectric, $\omega=ck/\epsilon^{1/2}(\omega)$, where k is the total wave vector. Alternatively, simple small-angle kinematics and the coherence condition of Čerenkov radiation give the equivalent relationship $\theta=[\beta^2\epsilon(\omega)-1]\hbar\omega/2E_0$, where E_0 is the energy and $\beta=v/c$ is the relativistic velocity of the electrons.

Figure 2(a) shows the energy-loss spectrum with foils tilted at 45° to the incident beam, where the tilt axis is perpendicular to the entrance slit of the spectrometer. As expected, the dispersion of volume losses, bulk plasmon and Čerenkov radiation, remain unchanged, whereas the dispersion of the surface plasmon has changed considerably.

In the following sections, quantitative data are presented in the course of a detailed examination

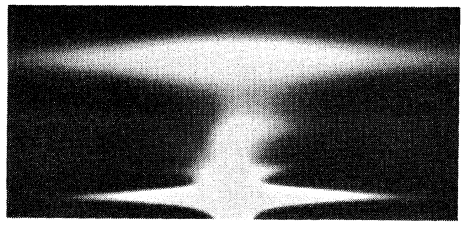

a

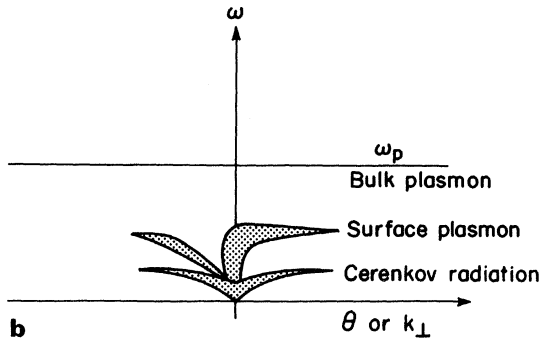

FIG. 2. (a) Electron energy-loss spectrum in silicon at 45° tilt. The change in surface plasmon dispersion is clearly visible, whereas the dispersion of Čerenkov radiation remains nearly unchanged. (b) A sketch of main features in (a).

of these losses in which effects due to the finite thickness of the sample are explored.

IV. VOLUME LOSSES: THEORETICAL BACKGROUND

Our concern is primarily with the energy-loss probability function $P(\omega, k_\perp)$, where $k_\perp$ is the component of the wave vector of the scattered electron perpendicular to the incident velocity of the electron. For high-energy electrons, small angle scattering, and small energy losses, $|k_\perp|$ is equal to $k_0\theta$, where k_0 is the incident electron wave vector. We do not reproduce the full expression for $P(\omega, k_\perp)$ here [see Eq. (26) of Kröger[3]; also Daniels *et al.*[4]], but various special cases for the volume and surface expressions are discussed. The volume loss is given by

$$\frac{\partial P_v(\omega, k_\perp)}{\partial\omega\,\partial^2 k_\perp} = \frac{e^2}{\pi^2\hbar v^2}\, 2a\,\mathrm{Im}\left(\frac{\mu^2}{\epsilon\phi^2}\right) , \qquad (1)$$

where e and v are the charge and velocity of the incident electron and $2a$ is the thickness of the foil. $\partial^2 k_\perp$ is the infinitesimal area element in the reciprocal lattice plane containing $k_\perp$. The parameters $\mu^2 = 1-\epsilon\beta^2$ ($\beta = v/c$) and $\phi^2 = \alpha_3^2 + \omega^2/v^2$ are complex quantities, where $\alpha_3^2 = k_\perp^2 - \epsilon\omega^2/c^2$. For large scattering angles or for infinite c (no retardation), Eq. (1) reduces to the expression originally derived by Ritchie[2]:

$$\frac{\partial P_v(E,\theta)}{\partial E\,\partial\Omega} = 2a\left(\frac{e}{\pi\hbar v}\right)^2 \mathrm{Im}\left(\frac{1}{\epsilon}\right)(\theta^2+\theta_E^2)^{-1} . \qquad (2)$$

In Eq. (2), the scattering probability has been rewritten in terms of the energy loss $E = \hbar\omega$ and an infinitesimal solid scattering angle $d\Omega$. Note that $k_0^2 d\Omega \equiv \partial^2 k_\perp$. Also, ϵ must be defined as $\epsilon_1 - i\epsilon_2$, $\epsilon_2(\omega) > 0$. The angle θ_E is defined as $k_\parallel/k_0$, where $k_\parallel = \omega/v$. The maximum in the energy-loss function, $\mathrm{Im}(1/\epsilon)$, gives rise to the bulk plasmon peak at ω_p.

The most significant difference between Eq. (1) and (2) occurs when the parameter ϕ^2 passes through a minimum. For real ϵ, the condition $\phi^2 = 0$ is satisfied for positive values of $k_\perp^2$ when $v > c/\epsilon^{1/2}$, which is the classical requirement for Čerenkov radiation. Then the dispersion relation is identical to the velocity of light line in an infinite dielectric, i.e., $k_\perp^2 + k_\parallel^2 = \epsilon\omega^2/c^2$ or $\omega = ck/\epsilon^{1/2}$, where $k = (k_\perp^2 + k_\parallel^2)^{1/2}$ is the magnitude of the total wave vector in the dielectric.

For complex ϵ, the conditions for radiation are somewhat less stringent. Equation (1) is equivalent to the form quoted by Festenberg and Kröger[11]

$$\frac{\partial P_v(E,\theta)}{\partial E\,\partial\Omega} = 2a\left(\frac{e}{\pi\hbar v}\right)^2 \times \mathrm{Im}\left(\frac{1}{\epsilon}\right)\frac{\theta^2+\theta_E^2[(1-\epsilon_1\beta^2)^2+(\epsilon_2\beta^2)^2]}{[\theta^2+\theta_E^2(1-\epsilon_1\beta^2)]^2+(\theta_E^2\,\epsilon_2\beta^2)^2} , \qquad (3)$$

which reduces to Eq. (2) for $\beta = 0$. A dispersion relation for $\theta_{\max}$, the Čerenkov peak is found by differentiating Eq. (3) with respect to θ:

$$\theta_{\max}^2 = \theta_E^2\left|\epsilon\beta^2 - 1\right|\left(\left|\epsilon\right|\beta^2 - \left|\epsilon\beta^2 - 1\right|\right) . \qquad (4)$$

There exist no positive values of $\theta_{\max}^2$ for $\epsilon_1\beta^2 < 0.5$. It can be shown that $\theta_{\max}$ is a monotonic increasing function of ϵ_2; as $\epsilon_2 \to \infty$, the upper bound on $\theta_{\max}$ is $\theta_E(\epsilon_1\beta^2 - \frac{1}{2})^{1/2}$. For $\epsilon_1\beta^2 > 1$ the lower bound on $\theta_{\max}$ as $\epsilon_2 \to 0$ is $\theta_E(\epsilon_1\beta^2 - 1)^{1/2}$ and, for $0.5 < \epsilon_1\beta^2 < 1$, the lower limit is $\theta_E[(\epsilon_1\beta^2 - 1)(1 - 2\epsilon_1\beta^2)]^{1/2}$. Then for $\epsilon_1\beta^2 \gg 1$, the position of the Čerenkov peak is controlled by ϵ_1, but the height and width of the peak depend on ϵ_2 [see Eq. (3)]. Below an absorption edge, the peak may become very narrow and intense as $\epsilon_2 \to 0$, but it is always limited to finite dimensions because ϵ_2 is never exactly zero. The location of the ridge of intensity in the E-θ plane is not rigorously defined by Eq. (4) when the Čerenkov peak is heavily damped ($\epsilon_2 \gg 1$). For silicon, the dispersion curve calculated from Eq. (4) has a negative gradient above the maximum of ϵ_1 (3.4 eV), but no such structure is visible in contour maps for the volume loss calculated from Eq. (1) because ϵ_2 is large above 3.4 eV. At large scattering angles the peak position defined by $\partial P_v/\partial E = 0$ is almost coincident with the interband tran-

sition at 3.4–3.5 eV. The effect of negative surface contributions to the intensity distribution in the volume plasmon and the Čerenkov peak is considered in Sec. VI.

V. SURFACE MODES: THEORETICAL BACKGROUND

The surface terms in the energy-loss probability function [Eq. (26) of Kröger[3]] all contain factors L^+ and L^- in the denominators, where

$$L^+ = \alpha_1\epsilon + \alpha_3 \tanh \alpha_3 a \quad , \tag{5a}$$

$$L^- = \alpha_1\epsilon + \alpha_3 \coth \alpha_3 a \quad . \tag{5b}$$

In these expressions, $\alpha_1 = (k_s^2 - \omega^2/c^2)^{1/2}$ and $\alpha_3 = (k_s^2 - \epsilon\omega^2/c^2)^{1/2}$ are the exponential decay constants of the fields in vacuum ($\epsilon_0 = 1$) and the dielectric slab (of thickness $2a$), respectively. For normal incidence k_s is identical to $k_\perp$. The two wave numbers are written with different subscripts to emphasize that k_s is confined to the surface plane. The dispersion of the surface plasmons is given by the location of minima in the functions $|L^+|$ and $|L^-|$ or equivalently by the maxima in $\mathrm{Im}(1/L^\pm)$. Then, for $k_s^2 \gg \omega^2/c^2$, $\epsilon\omega^2/c^2$, we obtain the standard expression for the energy dependence of the surface loss, $\mathrm{Im}(1/1+\epsilon)$. In practice, both definitions agree with the exact peak locations found by calculating the complete probability function. We note also that we are considering only p-polarized nonradiative modes.

In the simplest case of a free-electron metal ($\epsilon = 1 - \omega_p^2/\omega^2$), the equations $L^\pm = 0$ have solutions for $\epsilon \leq -1$. The asymptotic energy $\hbar\omega_s$ at large k_s occurs for $\epsilon = -1$. For thin films, the ω^+ mode has a higher energy, but both modes follow the light line $\omega \lesssim ck_s$ for small k_s.

Some qualitative ideas about the behavior of the surface modes in silicon can be obtained by considering a simple single-oscillator model for the dielectric constant where $\epsilon_1 = 1 + \omega_p^2/(\omega_T^2 - \omega^2)$ and $\epsilon_2 = 0$. The solutions where ϵ takes a similar form have been examined by Kliewer and Fuchs[14]; their results are summarized here. For $\omega > \omega_T$, ϵ is negative and approximately follows the free-electron case. The asymptotic energy $\hbar\omega_s$ is given by the condition $\epsilon = -1$. As ω approaches ω_T from higher energies, ϵ tends to $-\infty$ and both ω^+ and ω^- modes converge towards the light line. The free-electron model corresponds to the special case where $\omega_T = 0$.

Below ω_T, the solutions for the nonradiative modes (α_1 real) take a new form because α_3 is imaginary for $\epsilon\omega^2/c^2 > k_s^2$. The dispersion equations can be written

$$L^+ = \alpha_1\epsilon - \beta_3 \tan\beta_3 a \quad , \tag{6a}$$

$$L^- = \alpha_1\epsilon + \beta_3 \cot\beta_3 a \quad , \tag{6b}$$

where $\beta_3 = i\alpha_3$. For $\epsilon > 1$, $L^+ = 0$ has solutions for $(m-1)\pi/2 < \beta_3 a < m\pi/2$, where $m = 1$, 3, 5, etc., and L^- has solutions for $m = 2$, 4, 6, etc. Inside the dielectric, standing wave fields with a sinusoidal variation are set up. Unlike the solutions for $\epsilon < -1$, the internal fields do not decay exponentially away from the surfaces even for large values of $2a$. The situation corresponds to total internal reflection of travelling waves in a waveguide, where the fields outside the boundaries do not radiate but decay as $e^{-\alpha_1 z}$.

For both undamped and damped oscillators there are an infinite number of modes for $\omega \lesssim \omega_T$. With damping, the high-order modes will be heavily damped if ϵ_2 is large for $\omega \sim \omega_T$. Generally, the two types of internal wavefields are clearly separated only for small values of ϵ_2.

Without damping, the general properties of these modes as a function of the thickness $2a$ can be listed as follows: (i) all modes reach the light line $\omega = ck_s$, but the lowest-energy solution (ω_g^+ mode for $m = 1$ or $0 < \beta_3 a < \pi/2$) continues down to the origin; all other modes terminate at $\beta_3 a = (m-1)\pi/2$; (ii) for large k_s all modes are asymptotic to ω_T; (iii) at a given k_s, successive solutions at increasing energies alternate between ω_g^+ and ω_g^- modes; (iv) as $a \to 0$, the solutions all move upwards towards ω_T; (v) as $a \to \infty$, the curves spread out subject to a lower limit fixed by the velocity-of-light line in the dielectric, $\omega = ck_s/\epsilon^{1/2}$.

When damping is included in the single-oscillator model, the transition between the two types of wave field on either side of ω_T becomes blurred. The upper branch ($\omega > \omega_T$) does not simply terminate when ϵ_1 changes sign (at 4.3 eV in Si) as is implied by previous dispersion calculations[14,17] for real ϵ. Generally, the curves for $\mathrm{Im}(1/L^\pm)$ always include a peak at the light line for positive ϵ_1. Likewise, the exact solutions of $L^\pm = 0$, using a complex[18] ω and ϵ for a single damped oscillator, indicate that the curve for $\mathrm{Re}(\omega)$ lies slightly inside the light line, i.e., $\omega \geq ck_s$ for $\omega \geq \omega_T$. Above ω_T both methods of calculation yield identical results. The slight differences between these approaches are resolved when the complete distribution function for electron scattering is calculated. Then, for $\epsilon_1 \geq 0$, the highest peak intensities occur exactly on the light line, but there is an asymmetry towards higher energies. The same features are present on the Si contour maps (Figs. 3 and 4) and in similar maps for thick GaP films[3] ($2a = 3400$ Å), where the highest intensities are slightly inside the light line.

VI. INTERACTION OF SURFACE AND VOLUME EXCITATION

In Figs. 3 and 4 the probability distribution function for scattering of 75-keV electrons at normal incidence by a 1000-Å silicon film is plotted as a

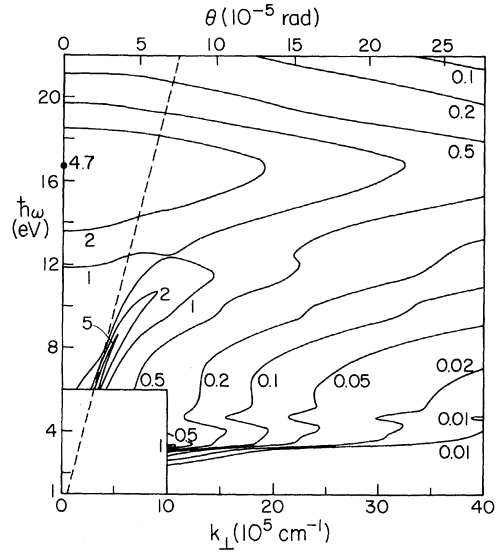

FIG. 3. Contour map for scattering of 75-keV electrons in a 1000-Å Si film. The figures on the contours refer to units of 10^5 eV^{-1} sr^{-1}, and the dashed line is the velocity of light line, $\omega = ck_\perp$.

contour map in the E-θ plane. The dielectric constants for Si are taken from recent optical measurements which are corrected for surface oxidation.[9] Values for ϵ_2 down to 1.1 eV are calculated from the curve for the absorption coefficient.

The positions of the surface modes follow the general principles discussed above. The dispersion of the surface plasmon above 5 eV corresponds to the peak of $\mathrm{Im}[(\alpha_1\epsilon + \alpha_3)^{-1}]$ because the ω^+ and ω^- modes are coincident. The peak is not well-defined for large k_s, i.e., away from the light line, partly because the width of the loss becomes comparable to the width of the volume plasmon[18] (~4 eV). The asymptotic energy $\hbar\omega_s$ is 11.6 eV ($\epsilon_1 \sim -1$). Below 4 eV there are three new surface peaks in addition to the primary loss which follows the light line. These are labeled (Fig. 5) as two ω_s^+ modes ($m = 1, 3$) and a ω_s^- mode ($m = 2$).[19] Their locations are identical to the peak positions calculated from $\mathrm{Im}(1/L^\pm)$. The upper bound for these excitations is set by the absorption edge at 3.3 eV (see Fig. 3).

The relationship of these peaks to the volume Čerenkov loss is perhaps best explored with the aid of Fig. 6, in which the scattering probabilities are plotted as a function of energy for several values of $k_\perp$. Above $k_\perp \approx 6.5\times10^5$ cm^{-1}, the volume loss dominates, whereas at smaller wave vectors the surface contribution, which is always negative at the Čerenkov peak, completely cancels out the volume term and the surface modes dominate. Mathematically, the presence of the parameter ϕ^2 in the denominators of both the volume term and the surface terms is responsible for this effect. The minimum value of $k_\perp$ for which the Čerenkov peak exists is approximately equal to π/a, i.e., $\lambda_{max} \approx 2a$, where λ_{max} is the longest photon wavelength which is not damped by surface effects.

Turning now to consider the bulk plasmon excitation, the angular intensity distribution in the volume term at $\omega = \omega_p$ closely follows Eq. (2) because relativistic corrections are small for $\epsilon_1, \epsilon_2 \sim 0$, i.e., $\phi^2 \sim k_\perp^2 + k_\parallel^2$. However, the angular half-width of the volume plasmon is always less than $2\theta_E$ because the intensity distribution is modified by negative surface contributions,[20] except at $k_s = 0$, where all surface terms are zero. For $2a = 1000$ Å (Fig. 7), the intensity deficit reduces the width by 5%. For comparison, the curve for $2a = 100$ Å is included, where the narrow peak within the light line ($k_\perp = \omega_p/c$) corresponds to the radiative surface plasmon[3] for $\omega \geq \omega_p$.

The measured intensity distribution (normalized at $k_\perp = 0$) matches the theoretical width to within 3% (Fig. 7). The accuracy of the angular calibration (± 3%) is insufficient to check the effect of the surface terms.

VII. DISPERSION OF ČERENKOV AND SURFACE EXCITATIONS

Qualitatively, the position and visibility of the volume and surface losses in the energy-loss spectra (Fig. 1) agree quite well with the contour maps (Figs. 3 and 4), except that the fine structure below 4 eV is not resolved. In part this may be due to instrumental resolution, but the major problem is likely to be the variation in sample thickness. In

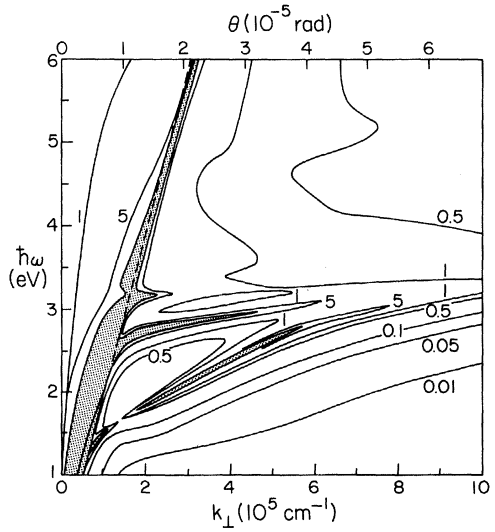

FIG. 4. Enlargement (4×) of area omitted in Fig. 3, showing the multiple surface modes at low energies and low wave vectors. The shaded areas correspond to intensities greater than 10 (units as in Fig. 3).

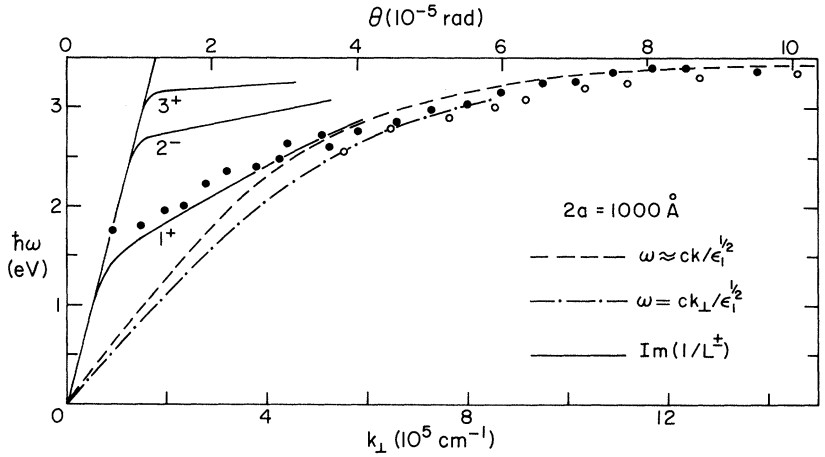

FIG. 5. Dispersion curves for the volume Čerenkov loss (dashed line) and the multiple surface losses (continuous lines). The surface modes $\omega_g^{\pm}(k_s)$ are labeled with the index m as 1^+, 2^-, and 3^+. The open and shaded circles represent experimental data for 45° tilt and normal incidence, respectively.

Fig. 8 the dispersion of the multiple-surface peaks is plotted for $2a = 2000$ Å. The lowest-order ω_g^+ mode now lies below the Čerenkov dispersion line and just above the lower limit $\omega = ck_s/\epsilon_1^{1/2}$(for $\epsilon_2 \simeq 0$). All other modes have also moved downwards, and there are three new peaks where the highest index ($m = 6$) corresponds to a ω^- mode. In general, as a increases, successive ω_g^+ and ω_g^- modes intersect the Čerenkov loss line. This effect is linked to the thickness-dependent oscillations in the photon emission curves calculated by Heitman.[10] For a wedge-shaped specimen, we must expect that the changing thickness will shift and blur the surface mode peaks—most likely into one very broad peak situated somewhere between $\omega = ck_s/\epsilon^{1/2}$ and $\omega \sim 3.2$ eV, as is indeed observed. For larger $k_\perp$ the peak intensity corresponds to Čerenkov radiation combined with interband losses.

The quantitative experimental evidence in support of this interpretation is given in Fig. 5. The measured dispersion fits the Čerenkov dispersion line closely for $\theta > 5\times10^{-5}$ rad, but at smaller angles the peak intensity moves into the region occupied by surface excitations. Also, the width of the peak increases at small angles and is not limited by the instrumental resolution.

Experiments with foils tilted at 45° to the incident beam, where the tilt axis is perpendicular to the entrance slit of the spectrometer, also suggest that the energy losses below 4 eV have a mixed surface and volume character. For a pure volume loss, the only effect of tilting the specimen is to increase the effective thickness, whereas for a surface loss k_s is confined to the plane of the film and the scattering probabilities for $\pm k_s$ are no longer equal. In addition the observed dispersion in the E-$k_\perp$ plane must be transferred back to the E-k_s coordinate system[21] before comparison with theory because $k_s \neq k_\perp$ for tilted films. In silicon foils, the dispersion of the surface plasmon above 4 eV is consistent with a simple surface excitation, but the lower loss does not show any measurable change in dispersion either for $\pm\theta$ or relative to the normal incidence data (Figs. 2 and 5). However, the peak heights for $\pm\theta$ are not exactly equal, particularly for small scattering angles close to

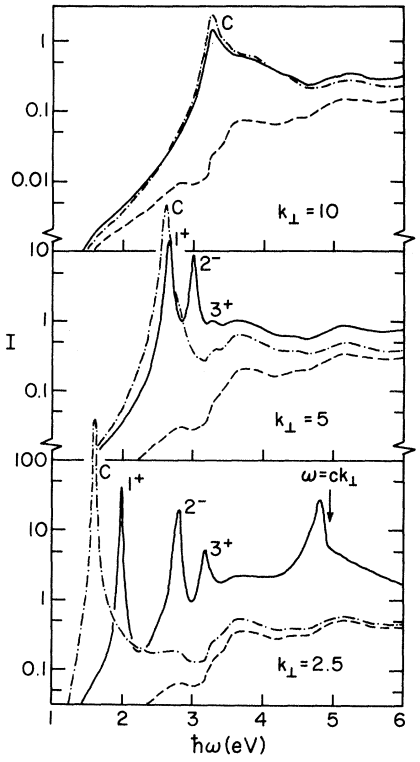

FIG. 6. Interaction of volume Čerenkov and surface peaks in Si ($2a = 1000$ Å) for several values of $k_\perp$ (units are 10^5 cm^{-1}). The intensity scale has units 10^5 eV^{-1} sr^{-1}. The dashed curves are the volume loss for $\beta = 0$ [see Eq. (2)], and the dot-dash curves represent the complete volume loss including the Čerenkov peak (labeled C). The solid curves are the total volume and surface energy-loss function, where the surface modes are identified as in Fig. 5.

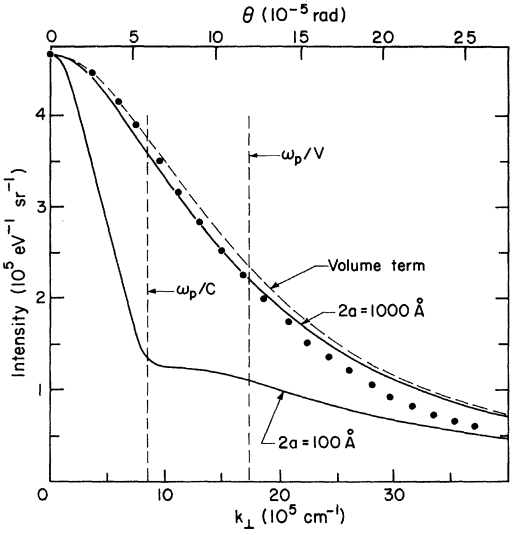

FIG. 7. Illustration of negative surface contributions to the angular intensity distribution in the volume plasmon (intensity for $2a = 100$ Å is multiplied by 10). The experimental data are normalized at $k_\perp = 0$. The angular resolution (8×10^{-6} rad) has no significant effect.

the light line. The sign of the asymmetry in the scattering probabilities matches the shift in the relative intensity of the surface plasmon peaks at higher energies (Fig. 2 and 9). Experiments with thin films grown by evaporation, i.e., with a uniform thickness, are needed to establish the behavior of surface losses for positive ϵ_1.

Normal incidence data for the dispersion of the surface plasmon above 4 eV are plotted in Fig. 10 for a Si foil with minimal exposure to the atmosphere (~ 15 min). Although the asymptotic energy is not measured, the data extend to 9.5 eV. After

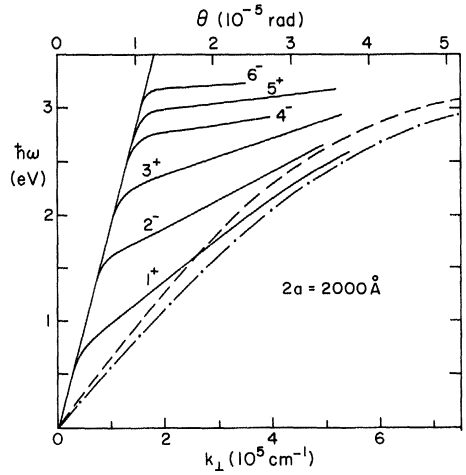

FIG. 8. Theoretical volume Čerenkov and surface dispersion curves for $2a = 2000$ Å (the curves are identified as in Fig. 5).

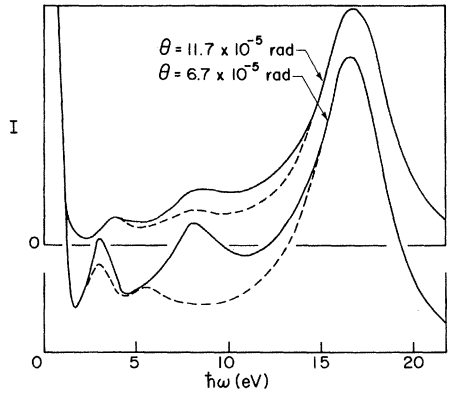

FIG. 9. Smoothed microdensitometer traces taken from the spectrum shown in Fig. 2(b) (45° tilt). Solid and dashed curves are for $\pm\theta$. For large θ, the intensities in the Čerenkov peaks at 3.4 eV are identical for $\pm\theta$, but at smaller angles the surface component affects the relative intensities. The same effects are seen in the surface plasmon at 8 eV, but the volume plasmon at 16.6 eV shows no asymmetries.

exposure to the atmosphere for several hours, i.e., sufficient time to form a relatively stable oxide layer, the dispersion was measured again with the foil tilted at 45° to the beam. Under these conditions, it is possible to measure $\hbar\omega_s$ because one branch has a much higher intensity. When the data are plotted in terms of ω and[21] k_s (Fig. 10), it can be seen that the dispersion does not match the normal incidence data. The asymptotic energy is 8.2 eV ($\hbar\omega_s = 11.6$ eV for clean Si).

Ideally, the surface-plasmon dispersion can be

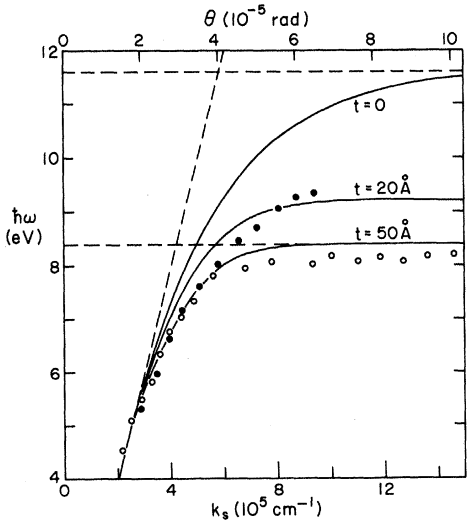

FIG. 10. Comparison of surface-plasmon dispersion (solid curves) calculated for several thicknesses (t Å) of silicon oxide (SiO_x). The filled circles represent normal-incidence data, and the open circles correspond to data transferred from 45°-tilt measurements.

used to measure the thickness of a contaminant layer, provided that all the dielectric constants are known. Unfortunately, most forms of surface contamination are specifically associated with the parent material, and are not necessarily identical in structure and composition with similar oxides, etc., grown by different methods. In the present case, the available dielectric data[22] for SiO, SiO_2 and SiO_x ($x \sim 1.5$) are used to make some approximate calculations about the composition and thickness of the surface oxide layer on silicon.

As a first step, the asymptotic energy is used to determine the composition of the oxide. An approximate condition for $\hbar\omega_s$ is that $\epsilon_1 = -\eta$, where η is the complex dielectric constant for the oxide layer. Then, for SiO, we find $\hbar\omega_s = 11.0$ eV and, for SiO_x and SiO_2, $\hbar\omega_s = 8.3$ eV. In the corrections made by Phillipp[8] for optical measurements on etched epitaxial Si films, a 15-Å SiO layer was used to fit the data. However, these results refer to short exposure times; for the purpose of the present calculations the composition SiO_x is assumed, and the thickness of the oxide layer is adjusted to fit the measurements.

The secular equation for the dispersion of surface charge oscillations at the interface between a semi-infinite slab and a superimposed layer with thickness t and dielectric constant η is given by[23]

$$L = \alpha_2\epsilon + \eta\alpha_3(1 - \gamma e^{-2\alpha_2 t})/(1 + \gamma e^{-2\alpha_2 t}) \ , \qquad (7)$$

where $\gamma = (\eta\alpha_1 - \alpha_2)/(\eta\alpha_1 + \alpha_2)$ and $\alpha_2 = (k_s^2 - \eta\omega^2/c^2)^{1/2}$. The data for a relatively clean surface (normal-incidence measurements) correspond to a 20-Å SiO_x layer, but a much larger thickness (> 50 Å) is required to fit the measured dispersion after a long exposure time (Fig. 10). These figures are not very accurate. The only definite conclusion is that η_1 for SiO is too small to account for the measured value of $\hbar\omega_s$, whereas η_1 for the higher oxides is consistent with our observations. Unfortunately, our present apparatus does not enable us to measure the dispersion curves at normal incidence and at 45° tilt without intermediate atmospheric exposure.

ACKNOWLEDGMENT

Professor J. Ballantyne kindly supplied us with material and advice on chemical thinning techniques.

*Work was supported by the Advanced Research Projects Agency and the National Science Foundation through the Materials Science Center at Cornell University.

[1]Optical experiments measure the transverse dielectric constant $\epsilon_t(k, \omega)$ at long wavelengths, whereas electron-energy-loss processes involve the longitudinal component $\epsilon_l(k, \omega)$ for volume excitations, and both ϵ_t and ϵ_l for surface excitations [see Fuchs and Kliewer (Ref. 18)]. The present measurements are confined to wavelengths in the optical range where the local approximation [$\epsilon_t = \epsilon_l = \epsilon(0, \omega)$] should be valid. Also, possible variations in ϵ due to crystal anisotropy are not considered here.

[2]R. H. Ritchie, Phys. Rev. 106, 874 (1957).
[3]E. Kröger, Z. Phys. 216, 115 (1968).
[4]J. Daniels, C. V. Festenberg, H. Raether, and K. Zeppenfeld, Springer Tracts Mod. Phys. 54, 77 (1970).
[5]J. J. Cowan and E. T. Arakawa, Phys. Status Solidi A 1, 695 (1970).
[6]R. B. Pettit, J. Silcox, and R. Vincent (unpublished).
[7]H. R. Philipp and H. Ehrenreich, Phys. Rev. 129, 1550 (1963).
[8]K. Zeppenfeld and H. Raether, Z. Phys. 193, 471 (1966); there exists some disagreement between various optical and electron-energy-loss measurements of $\hbar\omega_p$. The energy quoted here is an independent measurement.
[9]H. R. Philipp, J. Appl. Phys. 43, 2835 (1972).
[10]D. Heitmann, Z. Phys. 245, 154 (1971).
[11]C. V. Festenberg and E. Kröger, Phys. Lett. A 26, 339 (1968).
[12]C. V. Festenberg, Z. Phys. 214, 464 (1968); 227, 453 (1969).
[13]E. Kröger, Z. Phys. 235, 403 (1970).
[14]K. L. Kliewer and R. Fuchs, Phys. Rev. 144, 495 (1966).
[15]J. E. Lawrence and H. Koehler, J. Sci. Instrum. 42, 270 (1965).
[16]G. H. Curtis and J. Silcox, Rev. Sci. Instrum. 42, 630 (1971); P. E. Batson, J. Silcox, and R. Vincent (unpublished).
[17]J. Cazaux, Surf. Sci. 29, 114 (1972).
[18]R. Fuchs and K. L. Kliewer, Phys. Rev. B 3, 2270 (1971); this method for solving the secular equations $L^{\pm} = 0$ requires that ϵ be an analytic function because ω is a complex quantity. For the calculation mentioned in the text ϵ is written as $1 + \omega_p^2/(\omega_T^2 - \omega^2 + i\omega\gamma)$.
[19]The gap in the lowest-energy ω_g^+ mode (Fig. 4) can be traced to a negative contribution from the third surface term in $P(\omega, k)$ which contains a multiplying factor of β^4.
[20]H. Raether, Surf. Sci. 8, 233 (1967).
[21]A. Otto and J. B. Swan, Z. Phys. 206, 277 (1967); $k_\perp$ and k_s are related by the equation $k_s = k_\perp \cos\alpha + k_\parallel \sin\alpha$, where $k_\parallel = \omega/v$ and α is the angle of tilt. Here k_s and $k_\perp$ are written as scalars which may take positive or negative values.
[22]H. R. Phillipp, J. Phys. Chem. Solids 32, 1935 (1971).
[23]T. Kloos, Z. Phys. 208, 77 (1968).

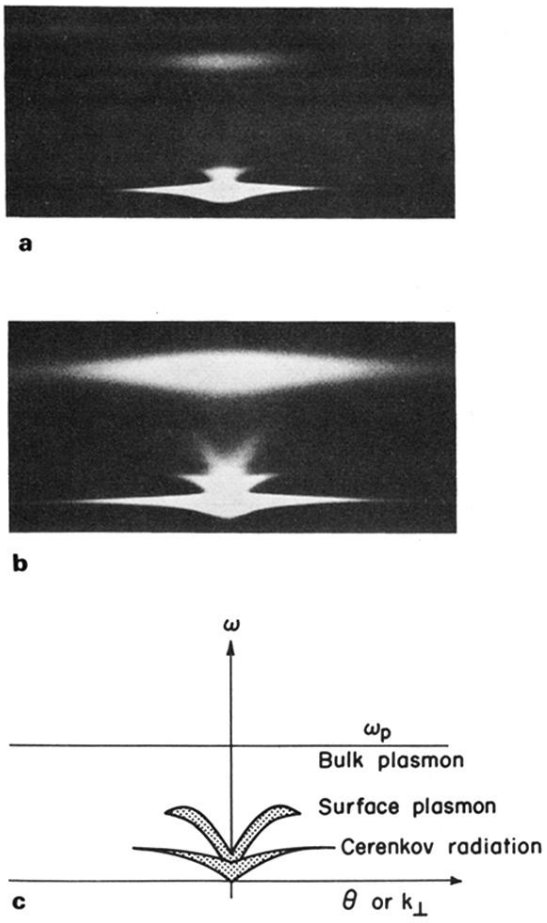

FIG. 1. Electron-energy-loss spectra in silicon at normal incidence. (a) Spectrum taken at lower exposure time (~4 min), in order to see the details close to the origin; (b) spectrum taken at longer exposure time (~10 min); (c) a sketch of main features shown in (a) and (b) with identification of losses. The horizontal line passing through the central spot ($\hbar\omega = 0$) contains electrons scattered by elastic collisions and by phonons.

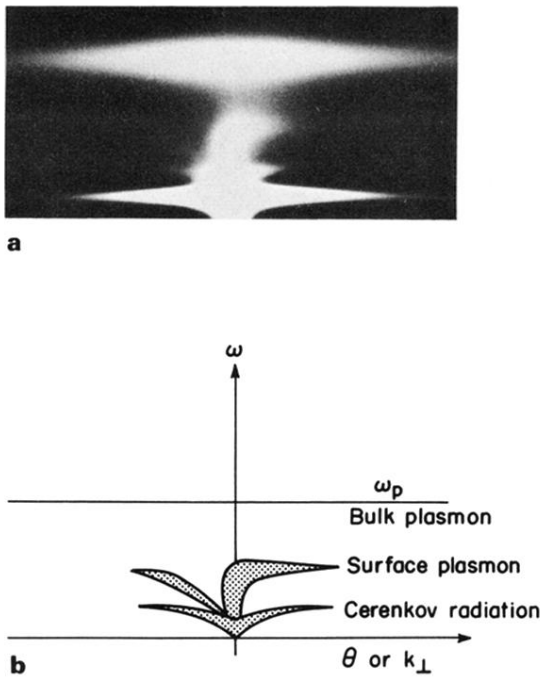

FIG. 2. (a) Electron energy-loss spectrum in silicon at 45° tilt. The change in surface plasmon dispersion is clearly visible, whereas the dispersion of Čerenkov radiation remains nearly unchanged. (b) A sketch of main features in (a).